A&A 506, 69–78 (2009)
DOI: 10.1051/0004-6361/200911678


Astronomy & Astrophysics
Special feature

*The CoRoT space mission: early results*

# Looking for pulsations in HgMn stars through CoRoT⋆ lightcurves

G. Alecian[1], M. Gebran[2], M. Auvergne[3], O. Richard[4], R. Samadi[3], W. W. Weiss[5], and A. Baglin[3]

[1] LUTH, Observatoire de Paris, CNRS, Université Paris Diderot, 5 place Jules Janssen, 92190 Meudon, France
e-mail: georges.alecian@obspm.fr
[2] Departament d'Astronomia i Meteorologia, Universitat de Barcelona, Mariti i Franques, 1, 08028 Barcelona, Spain
[3] LESIA, Observatoire de Paris, CNRS, 5 place Jules Janssen, 92190 Meudon, France
[4] GRAAL, Université Montpellier II, CNRS, Place Eugène Bataillon, 34095 Montpellier, France
[5] Institut für Astronomie (IfA), Universität Wien, Türkenschanzstrasse 17, 1180 Wien, Austria

Received 18 January 2009 / Accepted 7 May 2009

**ABSTRACT**

*Context.* HgMn chemically peculiar stars are among the quietest stars of the main-sequence. However, according to theoretical predictions, these stars could have pulsations related to the high overabundance of iron peak elements, which are produced by atomic diffusion in upper layers. Such pulsations have never been detected from ground-based observations.
*Aims.* Our aim is to search for signatures of pulsation in HgMn stars using the high quality lightcurves provided by the CoRoT satellite.
*Methods.* We identified three faint stars ($V > 12$), from a VLT-GIRAFFE multiobject spectrographic survey in a field planned for observation by CoRoT. They present the typical characteristics of HgMn stars. The three stars were observed by the CoRoT satellite during the *long run* (131 days) which started on 24 October 2007, with the exoplanets CCDs (Additional Programme). In the present work, we present the analysis of the ground-based spectra of these three stars and of the corresponding CoRoT lightcurves.
*Results.* Two of these three HgMn candidates show low amplitude (less than 1.6 mmag) periodic variations (4.3 and 2.53 days respectively, with harmonics) which are compatible with periods predicted by theoretical models.

**Key words.** stars: chemically peculiar – stars: oscillations – techniques: photometric

## 1. Introduction

HgMn stars are known to form a group among the chemically peculiar stars of the main-sequence (Preston 1974). Their photosphere is characterized by strong abundance anomalies of many metals (see for instance Castelli & Hubrig 2004). Overabundances with respect to solar ones can be about two orders of magnitude or greater. For instance, Mn can be enhanced by more than a factor of 200, and Hg by a factor of up to $10^6$. These stars are found in the range of effective temperature between about 10 000 K and 16 000 K (Pop I, B7-A0 IV-V), they are slow rotators, often binaries, and no associated magnetic fields have been detected (Shorlin et al. 2002; Wade et al. 2006). These stars, which are considered to have no convective motion in their atmosphere, do not show any indications of activity, and are among the quietest stars of the main sequence.

The trends of abundance peculiarities observed in HgMn stars are usually well understood in the framework of atomic diffusion (first proposed by Michaud 1970). As stated by the classical model, atomic diffusion builds up abundance stratification in the stable atmosphere (and envelope) of HgMn stars, according to the balance between radiative acceleration and gravity. Theoretical predictions by Alecian & Michaud (1981) for Mn are in excellent agreement with observations (Smith & Dworetsky 1993). However, modelling is not yet able to deal with the large variety of peculiarities observed in these stars. On the other hand, detailed studies of stratification build-up have not yet been done, because the numerical computations for optically thin media are very heavy (see Alecian & Stift 2007). Modelling of atomic diffusion in the stellar interior (the optically thick case) is more advanced (Richard et al. 2001). Even if these studies of stellar interiors cannot address the problem of atmospheric peculiarities, they allow one to better understand the evolution of these stars. Turcotte & Richard (2003) predict that, due to iron accumulation in the upper layers of their envelopes, these stars should at least be slow pulsators such as the slow pulsating B (SPB) stars. Presently, there is no observational evidence of pulsation in HgMn stars, and the CoRoT satellite offers an exceptional opportunity to constrain the models.

A detailed description of the CoRoT mission can be found in the *CoRoT book* (Baglin 2006) and Auvergne et al. (2009). Beside the two CCDs devoted to asteroseismology[1], the exoplanet CCDs photometrically monitor thousands of stars in the magnitude range $10.5 \leq m_R \leq 16$. This monitoring is designed to detect planet transits but is also interesting for studies of stellar photometric variations. Stellar scientists outside the CoRoT core programme are allowed to access the data of the exoplanet channel through the *Additional Programme* procedure (Weiss 2006).

In Sect. 2 we present our strategy to find, through ground-based observations (discussed in Sect. 3), faint HgMn stars in fields observed by CoRoT. In Sect. 4, we present the analysis

⋆ The CoRoT space mission was developed and is operated by the French space agency CNES, with participation of ESA's RSSD and Science Programmes, Austria, Belgium, Brazil, Germany, and Spain.

[1] Each of these CCDs, can measure photometric variation of 5 bright stars ($m_V < 9.5$)

of the CoRoT data for the targets we identified as HgMn candidates. In Sect. 5, we describe theoretical models for HgMn stars, followed by a discussion of our observational results.

## 2. Observational strategy

According to our knowledge of the solar neighborhood, we can estimate that about 8% of main-sequence AV-BV stars are HgMn stars. Therefore, applying this rate to the density of main-sequence AV-BV stars predicted by the "Besançon" model of stellar population synthesis of the Galaxy (Robin et al. 2003), in the anticenter direction, only about 0.3% of Pop I stars of any type may be HgMn. Then, one can expect to find about 35 HgMn stars in a field containing 11 400 stars, which is approximately the number of stars monitored by exoplanet CCDs. The problem is that there is no available catalog of such faint HgMn stars, since the MK classification with a dispersion sufficient to recognize the HgMn signature has been carried out only for relatively bright stars.

Prior to the launch of CoRoT, we have carried out a survey in fields pre-selected for exoplanet searches in the direction of the galactic anticenter, and using VLT-FLAMES/GIRAFFE (ESO) multiobject spectrograph.

The VLT-GIRAFFE 25' field towards the anticenter direction contains about 490 IV-V stars $11.5 \leq m_V \leq 16$, according to the "Besançon" model. The instrument can provide spectra of 110−120 objects in each field, with good enough resolution and $S/N$ to identify abundance peculiarities (see next section). If stars were selected at random, the probability of finding HgMn stars is extremely weak. To overcome this difficulty, we used a preliminary version of the *Exo-Dat* catalog (Deleuil et al. 2009), where the stellar types in our fields were approximately determined in view of the CoRoT mission, through multicolor broad band photometric observations by the CoRoT-Exoplanet team. The *Exo-Dat* catalog consists of 10.6 million stars over an area of 220 deg$^2$, observed with the Wide Field Camera (WFC) at the 2.5 m Isaac Newton Telescope (INT) at Roque Muchachos Observatory on La Palma, Canary Islands. Harris $B$ and $V$ filters and $r'$ and $i'$ filters from the Sloan-Gunn system were used (the limiting magnitude is about $r' = 20.0$). The spectral type, luminosity class and the mean reddening were obtained by fitting model atmospheres to the observed fluxes (Deleuil et al. 2009; Deleuil private communication). All stars classified as B0-A0 (IV-V), with low contamination[2], were systematically included in our programme, ensuring about 2 HgMn stars per set of targets. This programme was part of a larger one involving other teams[3].

## 3. Ground data

### 3.1. VLT-FLAMES/GIRAFFE observations

Observations were obtained during period 74A (0.5 night, 30, 31 January 2005), in the framework of the Paris Observatory GTO. In the present work, we use the data obtained in MEDUSA mode with setup LR02 (396.4−456.7 nm, $R = 6400$). Observational conditions were rather good with an average seeing of 0.6″−0.9″. Two exposures of 30 min were obtained for each field and an average $S/N$ of about 70 was reached for brightest targets. The spectra we use in this work were obtained after data reduction performed with the dedicated software GIRBLDRS developed at the Geneva Observatory[4]. Several tasks of the IRAF package for extraction, calibration, and sky correction of the spectra were also used.

[2] Only stars with low contamination are eligible for CoRoT observations. Contamination (by surrounding sources) is determined in *Exo-Dat* through criteria established for planet detection.

[3] 074.D-0193(A), *Looking deep in the CoRoT eyes*, G. Alecian (PI), A.-M. Hubert, M. Deleuil, C. Neiner, M. Floquet, C. Martayan.

**Table 1.** Programme stars and adopted effective temperatures, surface gravities and rotational velocities for our sample stars.

| Star | USNO-A2 | $m_V$ | $T_{\rm eff}$ (K) | log $g$ (dex) | $v_{\rm e} \sin i$ (km s$^{-1}$) |
|---|---|---|---|---|---|
| S1 | 0825-03036752 | 12.05 | 13 500 ± 500 | 4.00 ± 0.5 | 35 ± 5 |
| S2 | 0825-03028353 | 13.01 | 12 500 ± 500 | 4.50 ± 0.5 | 50 ± 8 |
| S3 | 0825-02993210 | 13.18 | 11 750 ± 500 | 4.00 ± 0.5 | 50 ± 8 |

### 3.2. Looking for HgMn stars

About 240 stars were observed in this run, and about 60 of them were classified in *Exo-Dat* as B0-A0 (IV-V) stars. To find HgMn candidates among these 60 stars, we searched for the characteristic pattern formed by two MnII lines (420.53 nm and 460.637 nm). This pattern is clearly visible in the spectra of HD 175640 (a high $S/N$ UVES spectrum of this star was kindly communicated by Hubrig, see Castelli & Hubrig 2004), and remains clearly recognizable after degrading the $S/N$ to 100. After a close examination of the spectra of these 60 stars, one star (S1) was found to show MnII line pattern very similar to HD 175640 (degraded spectrum), and two other stars (S2 and S3) were found with the same pattern, but less clearly. The characteristics of these three stars are shown in Table 1: their number in the USNO-A2 catalog, the visual magnitude from *Exo-Dat*, and the fundamental parameters discussed in Sect. 3.3. A rough estimate of various line strengths for abundances in HgMn stars was made using the COSSAM code (Stift 2000), and we checked the consistency of our selection of HgMn candidates by considering the spectra at other wavelengths. These three stars were then proposed to be included in the target allocated to the APs (Weiss 2006).

The detailed abundance analysis of these three stars, in the next subsections, have confirmed their identification as good HgMn candidates.

### 3.3. Fundamental parameters

The effective temperatures ($T_{\rm eff}$) and surface gravities (log $g$) of the stars were derived by adjusting a grid of theoretical Balmer lines to the observed one. With a lack of photometric data, fundamental parameters can only be determined spectroscopically. By simultaneously varying $T_{\rm eff}$ and log $g$, we select the profile that best fits the Balmer lines. LTE model atmospheres were calculated using Kurucz's ATLAS12 code (Kurucz 2005), assuming a plane parallel geometry, a gas in hydrostatic and radiative equilibrium and a depth-independent microturbulence. Abundances can be adjusted individually in ATLAS12, which uses the Opacity Sampling technique for line opacity. The increment in $T_{\rm eff}$ and log $g$ was 500 K and 0.5 dex respectively. We have used SYNSPEC code (Hubeny & Lanz 1992) to compute the synthetic Balmer profiles in the wavelength range of GIRAFFE spectra ($\lambda$3950−4550 Å). $H_\gamma$ and $H_\delta$ were generated using the line broadening functions of Vidal et al. (1973). The solar abundances used in SYNSPEC and ATLAS12 are those

[4] http://girbldrs.sourceforge.net

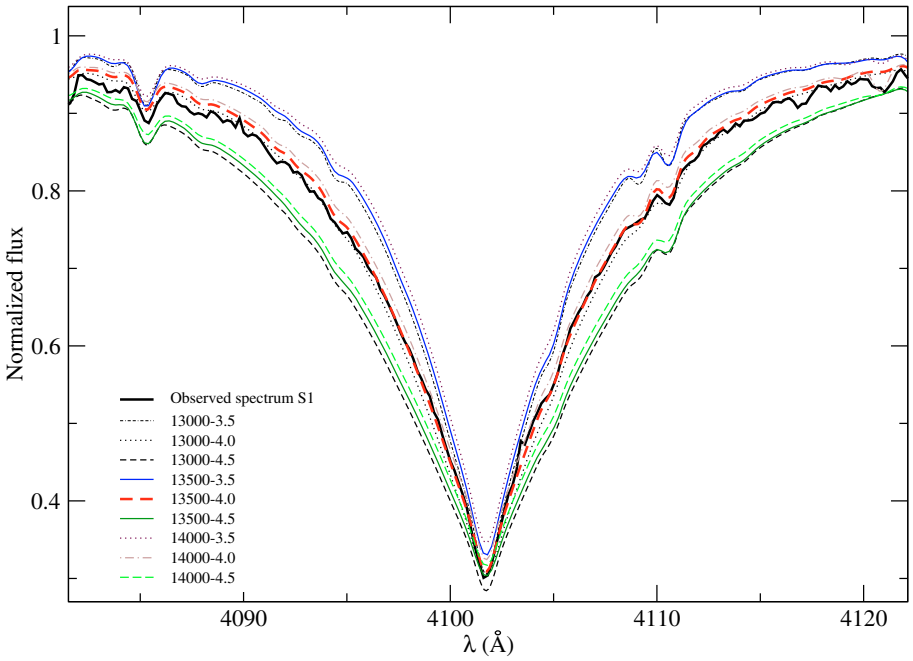


**Fig. 1.** The effect of changing $T_{\rm eff}$ by 500 K and $\log g$ by 0.50 dex on the spectrum around $H_\delta$. The adopted temperature and gravity for S1 are 13 500 K and 4.0 dex.

from Grevesse & Sauval (1998). These Balmer lines are computed using a non solar ATLAS12 model. After that, we select a model atmosphere, determine the abundances of the elements and these abundances are included in the new computed model atmosphere for the same star, the final models have the abundances displayed in Table 3.

For stars hotter than 8000 K, Balmer lines are more sensitive to gravity than to temperature. Figure 1 shows the effects of increasing and decreasing the effective temperature by about 500 K around 13 500 K on the profile of $H_\delta$. This variation of ±500 K corresponds to the estimated error on the effective temperature. In the same manner, we have tested the effects of changing the surface gravity by about ±0.50 dex, which is the estimation of the error bar on $\log g$. These tests were performed for the three stars and for both $H_\gamma$ and $H_\delta$ profiles. For stars earlier than mid-A type, hydrogen lines are relatively free from metal lines and thus an appropriate normalization to the continuum can be made. The adopted fundamental parameters are those of the model that best fit the overall shapes of Balmer lines. The adopted effective temperatures, surface gravities and rotational velocities are collected in Table 1 for S1, S2 and S3.

### *3.4. Abundance analysis*

#### 3.4.1. Input data

Once the fundamental parameters are fixed, the same ATLAS12 model atmospheres was as an input in the synthetic spectra calculations. We compiled a line list in the optical domain with the most accurate atomic parameters. For MgII, SiII, TiII, CrII, FeII, SrII and YII, we selected lines (Table 2) from the atomic transitions list of Gebran et al.'s (2008) online table, after verifying that these lines are good enough for abundances determination in the case of late B-type stars (i.e. no blending and strong enough). These authors used Kurucz's gfall.dat[5] as the initial line list, and they modified the atomic parameters of the investigated chemical elements (wavelengths, excitation potential, oscillator strength and damping constants) by checking for more recent laboratory determinations (as in the NIST and VALD databases). For HeI, CII, PII, MnII and HgII, we used Kurucz's data list. The helium abundances were derived using two lines of HeI at $\lambda$4143.8 and $\lambda$4471.5 using the broadening table of Barnar et al. (1969). We also included data for hyperfine splitting for the selected transitions when relevant, in particular for MnII. The spectral resolution of the spectra and the effect of rotational broadening prevent us from detecting the signature of hyperfine splitting. Mercury abundance was derived using the line of HgII at 398.39 nm with the oscillator strength from Sansonetti & Reader (2001).

#### 3.4.2. The method

Our main interest in the abundance determination is to detect HgMn features because we cannot derive accurate chemical abundances using low resolution spectroscopy and low signal-to-noise ratio spectra. We have derived individual chemical abundances of He, C, Mg, Si, P, Ti, Cr, Mn, Fe, Sr and Y by iteratively adjusting synthetic spectra to the observed normalized spectra. The synthetic spectra were computed using Takeda's (1995) code. Takeda's procedure iteratively minimizes the chi-square statistic between the synthetic spectrum and the observed one (see Takeda 1995 for a full description of the method).

The apparent rotational velocity ($v_{\rm e} \sin i$) and microturbulent velocity ($\xi_t$) were derived using the strong MgII triplet at 4480 Å and a set of neighboring unblended weak and moderately strong FeII lines between 4490 and 4530 Å as described in Sect. 3.2.1 of Gebran et al. (2008). Allowing small variations around solar abundances of Mg and Fe, we iteratively fitted these lines leaving $v_{\rm e} \sin i$ and $\xi_t$ as free parameters. The weak Fe II lines are sensitive to rotational velocity and not microturbulent velocity; the moderately strong FeII lines are sensitive to microturbulent velocity changes. The MgII lines are sensitive to both $v_{\rm e} \sin i$ and $\xi_t$. Each of the Mg and Fe lines yielded a set of values for $\log \epsilon$, $v_{\rm e} \sin i$ and $\xi_t$, which were in good agreement.

Once $v_{\rm e} \sin i$ and $\xi_t$ are fixed, abundances were derived for each line of each chemical element in our sample stars. With a resolving power of about 6500, errors on rotational velocities are approximately of the order of ~15%. Microturbulent velocities

[5] http://kurucz.harvard.edu/LINELISTS/GFALL/

**Table 2.** Detailed abundances (in $\log(N_X/N_H) + 12$ scale) for each line of each chemical element.

| Ion | $\lambda$ (Å) | $\log gf$ | S1 | S2 | S3 |
|---|---|---|---|---|---|
| HeI | 4143.800 | –1.19 | 9.486 | 9.177 | 9.500 |
| HeI | 4471.500 | 0.05 | 9.456 | 9.800 | 9.450 |
| CII | 4267.261 | –0.58 | 7.906 | 7.180 | 7.804 |
| MgII | 4390.510 | –1.70 | 6.975 | 7.359 | 7.122 |
| MgII | 4427.994 | –1.20 | 7.270 | – | 7.002 |
| MgII | 4481.10 | 0.73, –0.57, 0.57 | 7.201 | 6.720 | 7.154 |
| SiII | 4128.054 | 0.30 | – | 7.090 | 7.704 |
| SiII | 4130.894 | 0.46 | 7.857 | 6.702 | 7.350 |
| PII | 4420.712 | –0.48 | 7.608 | – | – |
| PII | 4452.472 | –0.19 | 7.420 | – | – |
| PII | 4466.140 | -0.28 | 7.437 | – | – |
| PII | 4468.000 | -0.21 | 7.760 | – | – |
| PII | 4475.270 | 0.30 | 7.670 | – | – |
| PII | 4483.693 | –0.43 | 7.502 | – | – |
| TiII | 4163.644 | –0.13 | – | 6.130 | 5.880 |
| TiII | 4287.873 | –1.79 | – | 6.206 | 5.340 |
| TiII | 4300.042 | –0.44 | – | 6.207 | 5.246 |
| TiII | 4386.844 | –0.96 | – | – | 5.293 |
| TiII | 4394.059 | –1.78 | – | 6.290 | 5.450 |
| TiII | 4395.051 | -0.54 | – | – | 5.270 |
| TiII | 4399.772 | –1.19 | – | 6.280 | – |
| TiII | 4417.714 | –1.19 | – | 6.180 | – |
| TiII | 4443.801 | –0.72 | – | 6.170 | – |
| CrII | 4616.629 | –1.29 | 6.740 | 5.510 | 6.113 |
| MnII | 4085.390 | –2.51 | 7.800 | – | – |
| MnII | 4252.963 | –1.13 | 7.820 | 7.180 | – |
| MnII | 4259.200 | –1.58 | – | 7.089 | 7.440 |
| MnII | 4292.237 | –2.22 | 7.310 | – | – |
| MnII | 4275.884 | –1.91 | 8.139 | – | – |
| MnII | 4278.614 | –2.51 | – | – | 7.080 |
| MnII | 4308.158 | –1.72 | – | 7.68 | 6.587 |
| MnII | 4310.692 | –0.15 | 7.677 | – | – |
| MnII | 4325.041 | –2.29 | 8.200 | – | 6.036 |
| MnII | 4356.621 | –2.02 | 7.809 | 7.246 | – |
| MnII | 4363.255 | –1.90 | 7.890 | 6.980 | – |
| MnII | 4478.637 | –0.95 | 8.040 | – | 6.708 |
| MnII | 4503.201 | –2.16 | 7.880 | – | – |
| MnII | 4518.965 | –1.32 | 7.850 | 6.900 | – |
| FeII | 4273.326 | –3.25 | 7.866 | 7.260 | 7.496 |
| FeII | 4296.570 | –3.01 | – | 7.380 | – |
| FeII | 4416.830 | –2.60 | 7.600 | – | – |
| FeII | 4491.405 | –2.70 | 7.887 | 7.106 | 7.123 |
| FeII | 4508.288 | –2.21 | 7.790 | 7.432 | 7.399 |
| FeII | 4515.339 | –2.48 | 7.860 | 7.510 | 7.349 |
| FeII | 4520.224 | –2.60 | – | 7.150 | 7.346 |
| FeII | 4522.634 | –2.03 | 7.760 | 7.520 | – |
| FeII | 4541.524 | –3.05 | 7.950 | – | – |
| NiII | 4067.031 | –1.83 | 5.463 | – | – |
| SrII | 4215.520 | –0.17 | 3.850 | – | 5.367 |
| YII | 4374.935 | 0.16 | – | 5.440 | 5.853 |
| HgII | 3983.90 | –1.51 | 7.700 | 7.200 | 6.065 |

**Table 3.** Abundances (relative to the sun) for S1, S2 and S3.

| Star | S1 | S2 | S3 |
|---|---|---|---|
| HeI | –1.53 | –1.51 | –1.17 |
| $\sigma_{He}$ | 0.09 | 0.31 | 0.20 |
| CII | –0.57 | –1.30 | –0.68 |
| $\sigma_{C}$ | 0.20 | 0.20 | 0.20 |
| MgII | –0.39 | –0.50 | –0.45 |
| $\sigma_{Mg}$ | 0.13 | 0.32 | 0.07 |
| SiII | 0.35 | –0.61 | 0.02 |
| $\sigma_{Si}$ | 0.20 | 0.19 | 0.18 |
| PII | 2.16 | – | – |
| $\sigma_{P}$ | 0.12 | – | – |
| TiII | – | 1.23 | 0.43 |
| $\sigma_{Ti}$ | – | 0.05 | 0.19 |
| CrII | 1.10 | –0.121 | 0.48 |
| $\sigma_{Cr}$ | 0.20 | 0.20 | 0.20 |
| MnII | 2.51 | 1.83 | 1.42 |
| $\sigma_{Mn}$ | 0.23 | 0.25 | 0.47 |
| FeII | 0.40 | –0.10 | –0.08 |
| $\sigma_{Fe}$ | 0.14 | 0.16 | 0.13 |
| NiII | –0.75 | – | – |
| $\sigma_{Ni}$ | 0.20 | – | – |
| SrII | 0.92 | – | 2.44 |
| $\sigma_{Sr}$ | 0.20 | – | 0.20 |
| YII | – | 3.24 | 3.65 |
| $\sigma_{Y}$ | – | 0.20 | 0.20 |
| HgII | 6.61 | 6.11 | 4.97 |
| $\sigma_{Hg}$ | 0.20 | 0.20 | 0.20 |

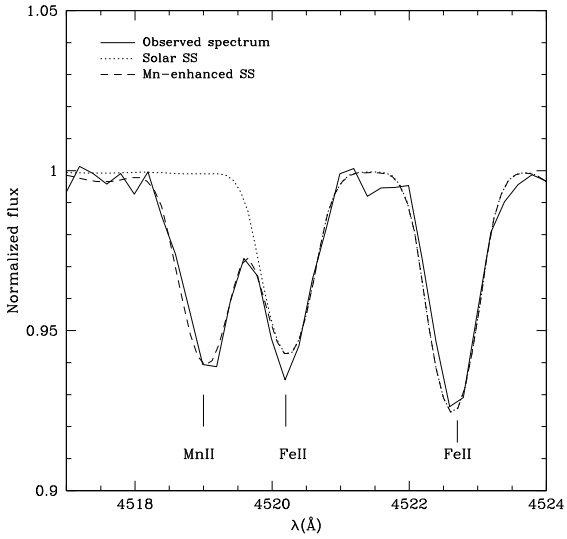


**Fig. 2.** Adjustment of synthetic spectra on the observed one for S1. The dotted lines represent a synthetic spectrum with solar abundance for all the elements. The dashed lines represent a synthetic spectrum with an enhancement of manganese by about 300 times the solar value.

were found to be very low, which is common in HgMn stars (see Smith & Dworetsky 1993), thus we decided to fix them to zero for S1, S2 and S3. The found apparent rotational velocities ($v_e \sin i$) are displayed in Col. 7 of Table 1.

The derived chemical abundances relative to the sun[6] for each line used for this analysis are shown in Table 2. The final abundances for each star, and their respective errors, are given in Table 3. The abundance [X/H] does not include the rescaling of the H abundance in order to account for the He deficiency.

[6] $\left(\left[\frac{X}{H}\right] = \log\left(\frac{X}{H}\right)_\star - \log\left(\frac{X}{H}\right)_\odot\right)$.

We have assumed that the abundances derived from several lines for a chemical element follow a Gaussian distribution. The errors on the element abundances are thus standard deviations. If the abundance is derived from only one line, we assign to it an error of 0.20 dex. We have also tested the effect on the derived abundance of changing the atmospheric parameters. Changing the effective temperature by ±500 K affect the mean derived abundances by ∼0.1−0.3 dex, depending on the element; the HgMn trends are not affected. Figure 2 displays an example of an iterative fitting of the MnII line at ∼4519 Å for S1. The synthetic spectrum with solar abundances is given by the dotted line

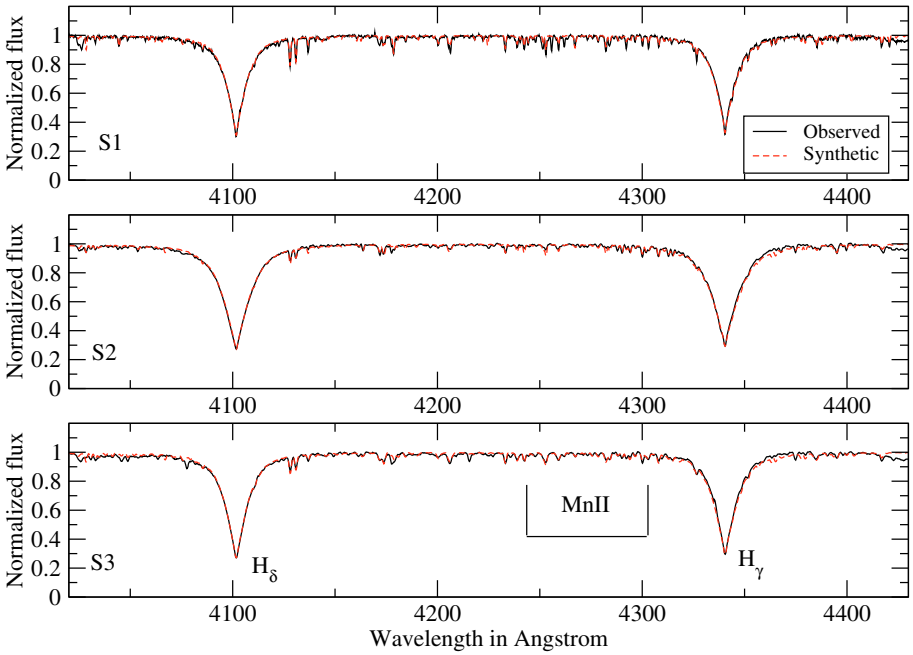


**Fig. 3.** Synthetic spectra superimposed on the observed ones for S1, S2 and S3. The range covers $H_\gamma$ and $H_\delta$ lines plus several manganese lines. The observed spectra are in the solid black line and the synthetic ones in the dashed red line.

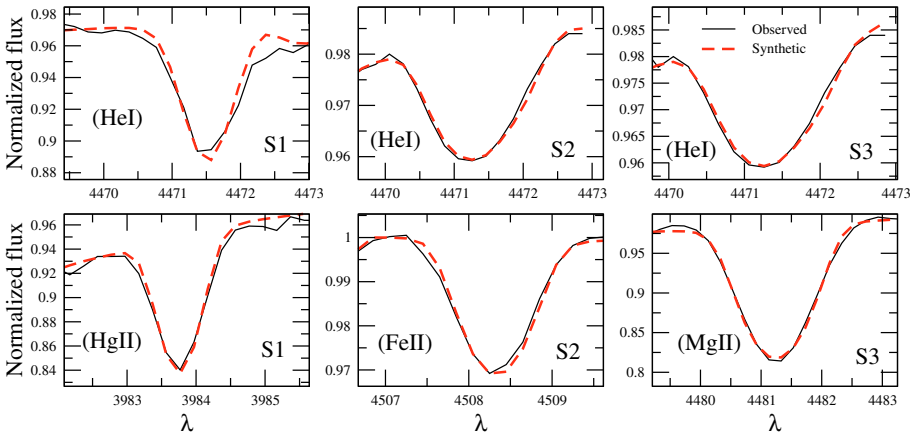


**Fig. 4.** Examples of line fitting using different chemical species for the three stars. Helium, mercury, iron and magnesium lines are displayed. The observed spectra are shown with the solid black line and the synthetic ones with the dashed red line.

and the manganese enhanced spectrum by the dashed line. In the case of S1, manganese is about 300 times higher than solar. In Fig. 3 we give the overall fit of the three stars between 4000 and 4400 Å. In this region, we have the two Balmer lines ($H_\gamma$ and $H_\delta$) and a large number of MnII lines. In Fig. 4, we show some examples of line fitting for S1, S2 and S3 and for several chemical elements such as He, Hg, Fe and Mg. Due to the low signal-to-noise ratio, some of the weak lines could not be analyzed such as titanium in S1 or nickel in S2 and S3. It is clear that all these 3 late-type B stars present HgMn features. Large overabundances are found for P, Mn, Sr, Y and Hg and underabundances in He and Ni. It also appears that the hotter HgMn star have a greater helium deficiency and manganese enhancement. Figure 5 displays the abundances pattern of S1, S2 and S3. One should be aware that the present analysis is based on low resolution and low signal-to-noise spectra, but the important result is that the HgMn pattern is clearly displayed in all three stars.

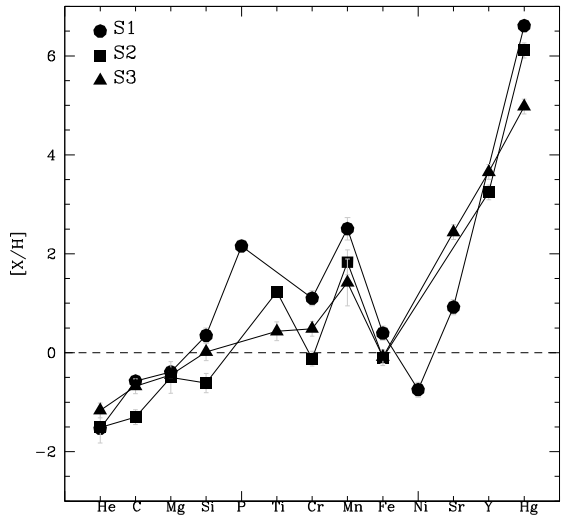


**Fig. 5.** Abundances pattern for our sample stars.

## 4. CoRoT observations

Stars S1, S2 and S3 were observed by CoRoT during the first *long run* towards the galactic anticenter (LRa01). This *long run* lasted from the 24th October 2007 to the 3rd March 2008, i.e. about 130 days. The results presented here are based on the *N2 data* provided by the CoRoT data center[7], released on October 29th, 2008. We carried out additional treatment of the

[7] http://idoc-corot.ias.u-psud.fr/index.jsp

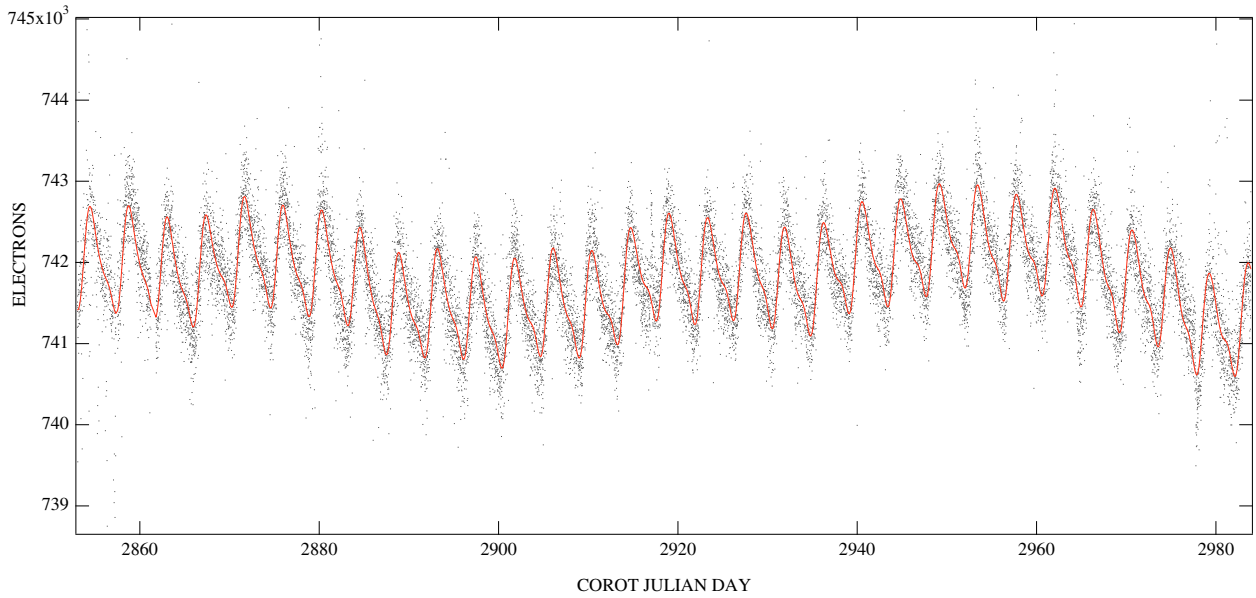


**Fig. 6.** S1 *white* lightcurve and the fit obtained using the frequencies of Table 4 (ELECTRONS vs. CoRoT JD).

data (see Sect. 4.1) using IgorPro v6 (from *Wavemetrics*)[8], and *Period04* v1.0.4 (Lenz & Breger 2005) for the analysis of frequencies.

For conciseness, in this section we will present in detail the treatment of data for the star S1 only.

### 4.1. Data preparation

A detailed presentation of the CoRoT data is given by Auvergne et al. (2009). For each of our three stars, CoRoT provided chromatic lightcurves, in the oversampled mode (32 s)[9]. These chromatic lightcurves are not able to give color information on targets, because the separation between the colors (which is carried out by the ground-based data processing) is arbitrary. Color separation was implemented to help in transit detection of exoplanets, but does not give workable information on a star's properties, at least at the present stage of data treatment. The colored fluxes are strongly sensitive to depointing fluctuations and consequently the jitter corrections on colors are not very efficient. The white light flux is less sensitive to jitter because the PSF slope is small on the aperture edges. Thus we first perform detection on white lightcurves.

The original set of *N2* lightcurves (red, green, and blue) for S1 consists of 338 729 points of measurement (electrons vs. CoRoT-Julian days), corrected for the main instrumental effects. We first selected the points flagged as "valid" (status = 0) by the *N2* pipe-line. Other points are generally affected by the so-called SAA (South Atlantic Anomaly) and/or other instrumental effects. However, some abnormal points survive this selection and need to be suppressed manually. At the end of this selection, we had 300 029 points of measurement (over 131 days). Most of them (98%) are spaced by 32 s, but the selection process introduces some gaps, often shorter than about 1100 s due to SAA. The SAA is crossed by the satellite 8 time per day, and lasts about 10 mn. There are also gaps due to interruptions (normal and abnormal) in data acquisition. The largest gap is 13.7 h from JD = 2861.23 due to missing data. The next step consisted of correcting the monotonic long-term variation of each curve by a parabolic fit. This variation is partly due to pointing shift, and partly due to instrumental drift. After this correction, we had three lightcurves; (average level, standard deviation) Red (391.373 kE, $\sigma$ = 1.293 kE), Green (107.826 kE, $\sigma$ = 0.435 kE), Blue (242.617 kE, $\sigma$ = 1.056 kE). To analyse frequencies (Sect. 4.2), we built the *white* lightcurve by simply summing the three chromatic lightcurves, and we achieved a binning of 512 s to reduce the noise (hereafter, all the plots and results are based on data with a binning of 512 s). A similar treatment was done for stars S2 and S3.

### 4.2. Data analysis and results

#### 4.2.1. Star S1

The *white* lightcurve (points) is shown in Fig. 6. The solid line is the fit obtained with Period04, using the frequencies listed in Table 4. This list of frequencies corresponds to frequencies with the highest amplitudes, from which the well-known CoRoT-orbital ones and their harmonics were removed. The full spectrum is shown in Fig. 7. The CoRoT orbital frequency at 13.97 c/d (161.7 $\mu$Hz) and its harmonics are clearly visible. The low frequencies around 0.01 c/d are related to the long-term variation noticeable in Fig. 6. We cannot interpret with certainty these long-term variations, which have periods comparable to the run duration. They do not correspond to known instrumental effects. Figure 8 presents the detailed spectrum around 0.23 c/d. The features around the peaks are due to the spectral window. In our opinion, the period $P \approx 4.3$ days, with two harmonics ($P/2$, $P/3$) is an intrinsic variation of star S1 and its amplitude ($\Delta m/m$) can be estimated to be about 1.6 mmag. There are no known CoRoT-periods around $P$, $P/2$ and $P/3$. This is easily visible in Fig. 6 (the "high" frequency variation).

#### 4.2.2. Star S2

The lightcurves of star S2 are much noisier than those of star S1. In addition, the blue lightcurve presents some strong discontinuities and perturbations from JD $\approx$ 2931.36. We therefore selected only points between JD = 2853.036 and 2931.35.

[8] http://www.wavemetrics.com/

[9] Chromatic and oversampled data are available only for a limited number of targets of the exoplanet channel.

**Table 4.** List of frequencies for star S1 (from Period04), used to calculate the fit of Fig.6.

| N | c/d | $\mu$Hz | Ampl. | Phase | Period (days) |
|---|---|---|---|---|---|
| 1 | 0.0114 | 0.132 | 413.9 | 0.7943 | 88.007 |
| 2 | 0.0146 | 0.169 | 106.3 | 0.8962 | 68.412 |
| 3 | 0.0251 | 0.290 | 174.6 | 0.0849 | 39.880 |
| 4 | 0.0436 | 0.505 | 74.1 | 0.7371 | 22.913 |
| 5 | 0.0877 | 1.015 | 73.5 | 0.4033 | 11.401 |
| **6 (P)** | 0.2324 | 2.689 | 552.9 | 0.9211 | 4.304 |
| **7 (P/2)** | 0.4648 | 5.379 | 212.7 | 0.6286 | 2.152 |
| **8 (P/3)** | 0.6982 | 8.081 | 37.1 | 0.5796 | 1.432 |

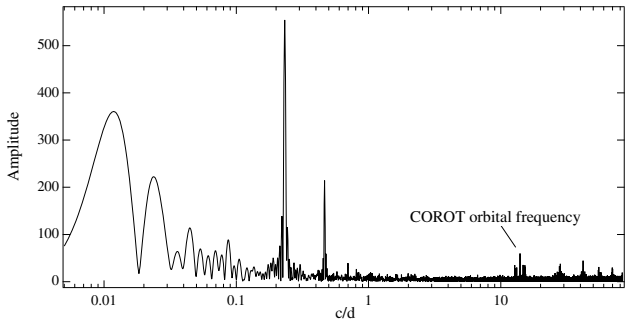


**Fig. 7.** Full S1 spectrum (amplitude vs. cycles per day) calculated with Period04 from the *white* lightcurve.

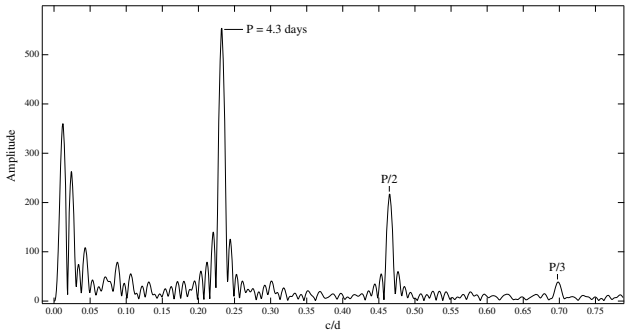


**Fig. 8.** Details of S1 spectrum. Zoom of Fig. 7, with a linear scale.

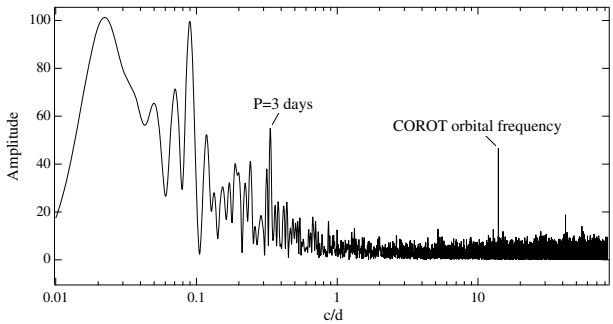


**Fig. 9.** Full S2 spectrum (amplitude vs. cycles per day) calculated with Period04 from the *white* lightcurve.

These data lead to the rather noisy spectrum shown in Fig. 9. Again, the CoRoT orbital frequency (and harmonics) dominates at 13.97 c/d (and above). The only other significant peak is for $0.337 \pm 0.01$ c/d, very close to a period of 3 days, which may be related to the 1 day period often present in CoRoT data. From these rather poor data, we cannot identify confidently frequencies intrinsic to the star S2.

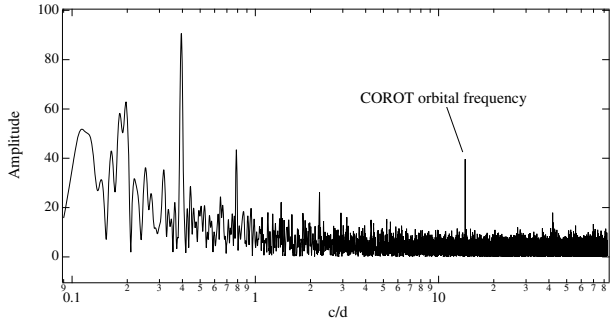


**Fig. 10.** Full S3 spectrum (amplitude vs. cycles per day) calculated with Period04 from the *white* lightcurve.

#### 4.2.3. Star S3

As in the previous case, lightcurves of star S3 present several discontinuities and perturbations, but not exactly at the same dates. However, compared to star S2, the lightcurves are less noisy and present interesting features. We considered the data between JD = 2853.036 and 2925.933 (73 days) and we show the corresponding full spectrum in Fig. 10; the details in the low frequency range (<3 c/d, linear scale) are given in Fig. 11. There are clearly two peaks above the noise, the first one at $0.395 \pm 0.01$ c/d ($P \approx 2.53$ days) and the second one at $0.789 \pm 0.01$ c/d, which is possibly the first harmonic (P/2). There is a peak around 0.19 c/d, but as one can see in more detail in Fig. 10, it does not emerge from the surrounding patterns as clearly as the previous peaks. Another isolated peak emerges around 2.24 c/d (0.446 day), but it seems less significant than the ones at 0.395 and 0.789.

## 5. Theoretical models for HgMn stars

The models for this paper are calculated with atomic diffusion that is known from first principles. In radiative zones this implies taking into account atomic diffusion including gravitational settling, thermal diffusion and radiative accelerations, in addition to the purely diffusive term. The interactions between different diffusing species are also taken into account. Convection and semi-convection are modeled as diffusion processes as described in Richer et al. (2000) and Richard et al. (2001). The detailed treatment of atomic diffusion is described in Turcotte et al. (1998). In these models, the Rosseland opacity and radiative accelerations are computed at each time step in each layer for the exact local chemical composition using monochromatic opacities of the OPAL group (Iglesias & Rogers 1996). The radiative acceleration for each element is from Richer et al. (1998) with correction for redistribution of momentum to electrons and others ions from Gonzalez et al. (1995) and LeBlanc et al. (2000). All models have an initially homogeneous solar composition.

For this preliminary study, we include mixing in all the models in an ad-hoc parametric way as in Richer et al. (2000), where the parameters specifying effective transport coefficients are defined. All our models were computed with a effective transport coefficient, $D_T$, 50 times larger than the He atomic diffusion coefficient at $\log T = 5.3$ and varying as $\rho^{-3}$ deeper in the star (for temperatures below $\log T = 5.3$ we assume complete mixing). The choice of the layer with $\log T = 5.3$ as a lower boundary of the mixed zone is justified by the fact that the iron accumulation (due to diffusion process) around those layers leads to the appearance of a convection zone. The existence of the HgMn phenomenon shows that full mixing cannot extend deeper, otherwise superficial abundance anomalies would not appear. According to the diffusion model, this lack of deeper

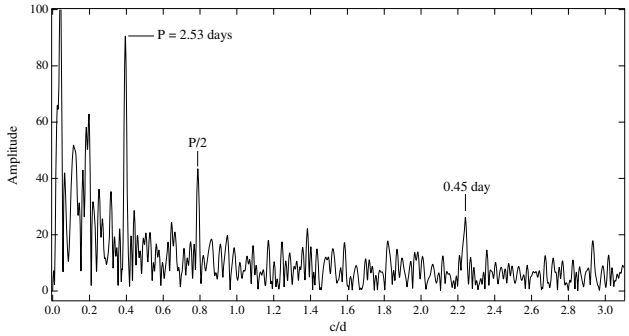


**Fig. 11.** Details of S3 spectrum. Zoom of Fig. 10, with a linear scale.

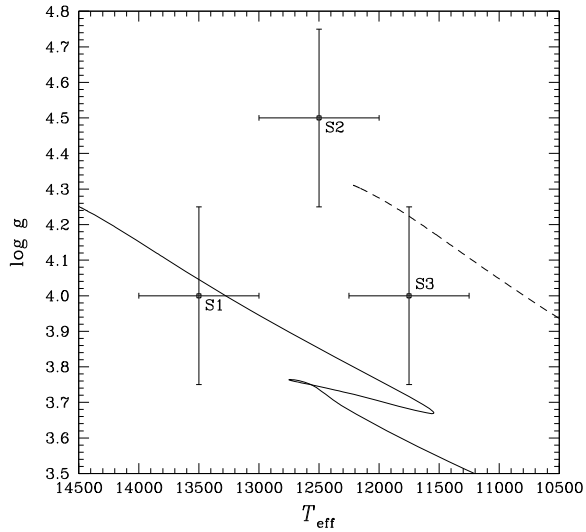


**Fig. 12.** Evolution of models of 3.0 $M_\odot$ and 4.0 $M_\odot$ in the $\log g - T_{\rm eff}$ plan. S1, S2 and S3 are shown with error bars.

mixing may be due to the slow rotation of HgMn stars. To better model HgMn stars, one would like to compute atomic diffusion in higher layers (with lower temperature, including the atmosphere). But the monochromatic opacities available to us are not sufficiently accurate to compute reliable radiative accelerations at low temperature (LeBlanc et al. 2000; Richer et al. 1998) and also, moving the boundary of the fully mixed zone to lower temperature leads to numerical difficulties in the present version of our code. Therefore, in our models, mixing impedes atomic diffusion in layers with $\log T < 5.3$. Notice that we have not adjusted the mixing depth to fit the surface abundances of our observed stars, because these anomalies are expected to be due to atomic diffusion in the atmosphere. For layers deeper in the star, where $\log T \geq 5.3$, the effective transport coefficient is adjusted to rapidly decrease the efficiency of the mixing, so in these layers the effect of atomic diffusion leads to chemical stratification and to an accumulation of iron, which affect the opacities and the pulsational properties of the models.

We have computed models of 3.0 $M_\odot$ and 4.0 $M_\odot$ which are in the mass range of S1 and S3 stars (see Fig. 12). As shown in Fig. 13, these models have a large bump in the opacity profile around $\log T = 5.3$; at this temperature radiative acceleration leads to an iron overabundance. In this region, see Fig. 14, oscillations could be driven by the $\kappa$-mechanism as $\frac{\rm d}{{\rm d}r}(\kappa_T + \frac{\kappa_\rho}{\Gamma_3 - 1}) > 0$, where $\kappa_T = (\partial \ln \kappa / \partial \ln T)_\rho$ and $\kappa_\rho = (\partial \ln \kappa / \partial \ln \rho)_T$.

The seismic properties of the models were studied with the *nadrot* code (Dziembowski 1977). Both the 3.0 $M_\odot$ and the 4.0 $M_\odot$ models show positive growth rates for non radial gravity

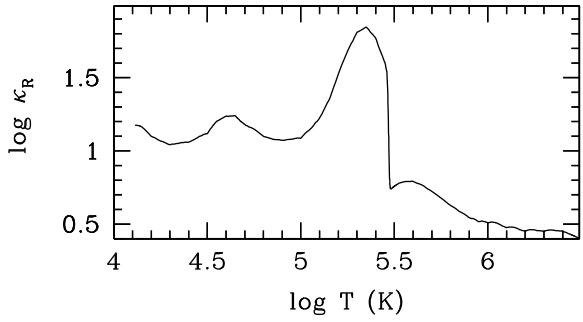


**Fig. 13.** Rosseland mean opacity versus temperature in the 4.0 $M_\odot$ model at the age of 100 Myr.

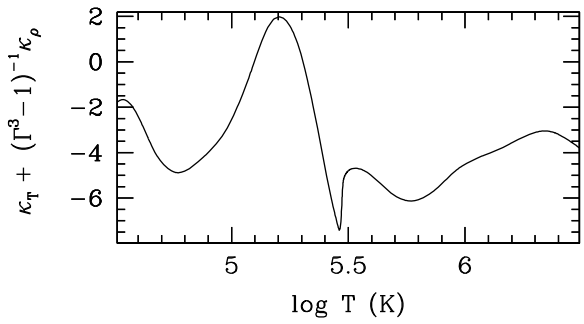


**Fig. 14.** Logarithmic opacity derivatives vs temperature for the 4.0 $M_\odot$ model at the same age as in Fig. 13.

modes, and all p-modes are stable. In the 4.0 $M_\odot$ model, the periods can be as short as 16 h and as long as 2 days for young models, whereas no mode under 33 h is overstable at the end of the main-sequence. The upper limit for the period, when the 4.0 $M_\odot$ stars leave the main-sequence, is hard to define, as the number of modes identified by the pulsation code is limited, but we find modes with periods as long as 4.4 days to be overstable, while modes with periods above 6.5 days are stable. The 3.0 $M_\odot$ model has a similar range in period for young models but shows a smaller shift to longer periods during evolution, with no overstable modes with periods longer than 2.5 days, until all modes become stable, around 250 Myr.

## 6. Discussion

The variations we find for stars S1 and S3 can be reasonably considered as intrinsic to these stars.

The VLT/GIRAFFE spectra used in this work are medium resolution spectra, thus the $v \sin i$ (Table 1) we obtained are not very accurate and rather can be considered as upper limits of the values one could expect to determine from higher resolution spectra. Since $v \sin i$ fixes a lower limit on the equatorial velocity, it gives an indication of the upper limit of the rotational period. The upper limits of the rotational period, which can be inferred from Table 1, appear to be in the same ranges as the periods we find for S1 and S3. Therefore, one cannot exclude at this stage that the variations found in our lightcurves are due to rotational modulation (see for instance Lanza et al. 2009).

### 6.1. Rotational modulation hypothesis

According to the discussion by Clarke (2003), surface inhomogeneities like spots or patches can produce photometric variations, but only the fundamental and the second harmonic can be present and not the third harmonic as we observe in S1. However,

it is difficult to assert that high degree harmonics cannot be found in a Fourier analysis in the case of complex superficial structures. Magnetic Ap stars are known to have large-scale and organized strong magnetic fields, with abundance patches of many metals. These anomalies are qualitatively well understood in the framework of atomic diffusion but the detailed quantitative modelling of that process is difficult, and sometimes strongly suggests that diffusion has to work with other processes like inhomogeneous winds (Babel 1992). A complete discussion should also consider light-induced drift and ambipolar diffusion. Such superficial structures have been studied for several decades from line shape variations (for recent studies, see for instance observations by Kochukhov et al. 2004; and modelling by Alecian & Stift 2007), and we would not be surprised if such complex structures cause photometric variations (in addition to those due to the roAp phenomenon for cool magnetic Ap stars). If our stars were not HgMn, but magnetic Ap stars, we would have carefully examined the role of rotational modulation to explain lightcurve variations.

Considering that the 3 stars discussed in this work are likely to belong to the HgMn group, is the hypothesis of abundance patches or spots relevant in explaining the photometric variations we observe? Observational facts are: there is not yet any confirmed detection of magnetic fields (Shorlin et al. 2002; Wade et al. 2006) nor any detection of photometric variation (Adelman et al. 2002) in HgMn stars from ground-based observations. There are some possible cases of a few hundred Gauss detections (Hubrig et al. 2006a), but they need to be confirmed, and they are not typical for the HgMn group. Following these constraints, standard diffusion modelling of HgMn stars consists of estimating the diffusion velocities and the resulting vertical stratifications of elements (equilibrium approximation), assuming stable atmospheres without magnetic fields. This modelling produced encouraging results by explaining the main trends of metal overabundances in these stars (Smith & Dworetsky 1993), but cannot yet reproduce the large variety of detailed observations of individual stars. An important reason for the difficulty in modelling individual stars is that diffusion is a slow[10] (and then sensitive) time-dependent process which, at a given time, has built up abundance stratifications which are different from those computed assuming equilibrium (the final stage of an ideal unperturbed time-dependent process).

Because, in the standard model, atomic diffusion is supposed to work alone, any perturbation, as could exist in a real HgMn star, can modify the stratification build-up process. For instance, effects induced by binarity, slow matter circulation, weak turbulence or wind can exist in HgMn stars. If so, they could be undetectable but be strong enough to affect the stratification. Among possible theoretical scenarios, one can consider the existence of weak, unorganized magnetic fields (hardly detectable). In magnetic Ap stars, where magnetic field strengths can be higher than several kG, the ion velocity component that is orthogonal to the field lines is significantly reduced above $\log\tau \approx 0$ and vanishes as the matter density decreases. This leads to the formation of non-uniform (horizontally) clouds of metals, anchored in the usual line-forming region (just above $\log\tau \approx 0$). In HgMn stars, if weak fields exist, the effect on diffusion velocities will be the same as in magnetic stars, but much higher in the atmosphere (for instance, above $\log\tau \approx -4.0$ for fields $\leq$1 kG, see Alecian & Stift 2006). This is due to the fact that the diffusion velocity of an ion in a magnetic field is slowed down by a factor that varies more or less as the square of the proton number density (see the detailed formulae in Sect. 4.1 of Alecian & Stift 2006). So, a weak magnetic field that will have no noticeable effect in usual line-forming regions could, however, force elements to remain bound to the star. In that case, one could expect that there may be additional high altitude clouds for some elements, forming abundance patches (related to the magnetic field orientation, possibly unorganized) and superimposed on the uniform stratifications predicted by the standard diffusion models.

Recent works (Adelman et al. 2002; Kochukhov et al. 2005; Hubrig et al. 2006b) have detected variations in some sparse line profiles in some HgMn stars and interpreted them in terms of abundance spots. As discussed, these observations are not necessarily in contradiction with the diffusion model. Moreover, these variations of line profiles are essentially found for elements having low cosmic abundances (Hg, Y, Pt, Zr), which give additional support to the diffusion model. Indeed, according to knowledge of radiative accelerations, these kinds of elements are generally strongly pushed up by the radiation field[11] and can more easily accumulate than abundant elements in the upper atmosphere (in addition to deeper stratification), where a weak magnetic field becomes able to impede atomic diffusion to expel that element toward the circumstellar medium.

According to the published profile variations mentioned above (the papers do not give any estimation of the photometric variations that can be induced by these profile variations), it is unlikely that, even if our stars would have the same kind of line profile variation, they could produce the 1.6 mmag photometric variations we observed in CoRoT lightcurves. The CoRoT lightcurves are integrated photon flux from about 400 nm to 1000 nm. To have regular photometric variations (as the ones we observed) from abundance spots, equivalent width of lines should vary more or less in phase. This is not observed and this is not consistent with abundance patches, which would be distributed differently for different elements. This does not mean that line profile variations could not coexist with photometric variations, rather, these two types of variations are related to two different mechanisms.

Our conclusion is that the variations observed recently in some sparse line profiles for some HgMn stars remain consistent with the diffusion model, but do not explain the photometric variations we observed in CoRoT lightcurves. Nevertheless, even if we think that these variations are not rotational modulations, more precise measurements of v.sini are clearly needed to discriminate between pulsations and rotational modulation, and to determine whether these stars are multiple or not. This is planned for the near future.

### 6.2. Pulsation hypothesis

In the hypothesis of pulsations, we have a significant 4.3 day period in S1, and 2.53 day period for S3. They are compatible with periods of non-radial g-modes predicted by models presented in Sect. 5. According to these models and the study of Turcotte & Richard (2003), these pulsations should be of the same type as those of SPB stars (Dziembowski et al. 1993). However, one cannot consider these stars as belonging to the SPB class, since stars of this class have more or less solar abundances. On average SPB stars are hotter than HgMn stars, and have higher gravity. However, the boundaries at the cool edge and at the low gravity edge of SPBs (De Cat 2007) overlap respectively the hot/large

[10] Diffusion time scales in atmospheres extend from some years to centuries according to the considered element.

[11] Because photoabsorption by bound-bound transitions remain unsaturated until very large overabundances are obtained.

ones of HgMn group. In the same way, the periods we find for S1 and S3 are slightly longer and with smaller amplitudes (less than or around 1.6 mmag) than what is generally found for SPBs, but here again these variations are compatible with those observed for some modes of SPBs. If pulsations were confirmed in the future in HgMn stars, differences could come from the lack of a superficial convection zone, which leads to strong metal stratification in the outer layers in HgMn stars(including the atmospheres). This could possibly cause stronger damping of those modes compared to SPB stars.

## 7. Conclusions

In this work, we first identified, from multiobject spectroscopy with moderate resolution (using VLT-GIRAFFE spectrograph), 3 faint stars presenting the characteristic features of HgMn types, and eligible for observation with the exo-CCDs of the CoRoT satellite. Their lightcurves, obtained during the run LRa01 of CoRoT, show periodic variations for at least two of theses stars. The periods of these variations are compatible with theoretical predictions. This could be the first detection of pulsation in HgMn stars. However, further ground-based high resolution spectroscopic observations are needed to confirm the HgMn nature of these stars and that these variations are pulsations and not rotational modulations.

*Acknowledgements.* The ground-based spectra used in this work are from a multi-purpose survey to prepare several CoRoT programmes. We would like to thank C. Martayan who obtained the observations corresponding to the anticenter direction with the (ESO) VLT/FLAMES-GIRAFFE spectrograph, for the data reduction and for his help during preparation of the survey. Thanks are also due to the CoRoT exoplanet team, and specially M. Deleuil, C. Moutou, and J. C. Meunier for having made available the necessary data of the Exo-Dat Catalog prior to its official release. We would like also to thank CNES (the French space agency) for a financial contribution.

## References

Adelman, S. J., Gulliver, A. F., Kochukhov, O. P., & Ryabchikova, T. A. 2002, ApJ, 575, 449
Alecian, G., & Michaud, G. 1981, ApJ, 245, 226
Alecian, G., & Stift, M. J. 2006, A&A, 454, 571
Alecian, G., & Stift, M. J. 2007, A&A, 475, 659
Auer, L. H., & Mihalas, D. 1973, ApJS, 25, 433
Auvergne, M., Bodin, P., Boisnard, L., et al. 2009, A&A, 506, 411
Babel, J. 1992, A&A, 258, 449
Baglin, A. 2006, The CoRoT mission, pre-launch status, stellar seismology and planet finding, ed. M. Fridlund, A. Baglin, J. Lochard, & L. Conroy, ESA SP-1306, ESA Publication Division (The Netherlands: Noordwijk)
Barnard, A. J., Cooper, J., & Shamey, L. J. 1969, A&A, 1, 28
Castelli, F., & Hubrig, D. 2004, A&A, 425, 263
Clarke, D. 2003, A&A, 407, 1029
De Cat, P. 2007, CoAst, 150, 167
Deleuil, M., Meunier, J. C., Moutou, C., et al. 2009, AJ, 138, 649
Dziembowski, W. 1977, Acta Astron., 27, 95
Dziembowski, W. A., Moskalik, P., & Pamyatnykh, A. A. 1993, MNRAS, 265, 588
Lenz, P., & Breger, M. 2005, CoAst, 146, 53
Gebran, M., Monier, R., & Richard, O. 2008, A&A, 479, 189
Gonzalez, J.-F., LeBlanc, F., Artru, M.-C., & Michaud, G. 1995, A&A, 297, 223
Grevesse, N., & Sauval, A. J. 1998, Space Sci. Rev., 85, 161
Hubeny, I., & Lanz, T. 1992, A&A, 262, 501
Hubrig, S., North, P., Scholler, M., & Mathys, G. 2006a, AN, 327, 289
Hubrig, S., González, J. F., Savanov, I., et al. 2006b, MNRAS, 371, 1953
Iglesias, C. A., & Rogers, F. J. 1996, ApJ, 464, 943
Kochukhov, O., Bagnulo, S., Wade, G. A., et al. 2004, A&A, 414, 613
Kochukhov, O., Piskunov, N., Sachkov, M., & Kudryavtsev, D. 2005, A&A, 439, 1093
Kurucz, R. L. 2005, Mem. Soc. Astron. It. Suppl., 8, 14
Lanza, A. F., Aigrain, S., Messina, S., et al. 2009, A&A, 506, 255
LeBlanc, F., Michaud, G., & Richer, J. 2000, ApJ, 538, 876
Preston, G. W. 1974, ARA&A, 12, 257
Richard, O., Michaud, G., & Richer, J. 2001, ApJ, 558, 377
Richer, J., Michaud, G., Rogers, F., et al. 1998, ApJ, 492, 833
Richer, J., Michaud, G., & Turcotte, S. 2000, ApJ, 529, 338
Robin, A. C., Reylé, C., Derrière, S., & Picaud, S. 2003, A&A, 409, 523
Sansonetti, C. J., & Reader, J. 2001, Phys. Scr., 63, 219
Shorlin, S. L. S., Wade, G. A., Donati, J.-F., et al. 2002, A&A, 392, 637
Smith, K. C., & Dworetsky, M. M. 1993, A&A, 274, 335
Stift, M. J. 2000, A Peculiar Newsletter, 33
Takeda, Y. 1995, PASJ, 47, 287
Turcotte, S., & Richard, O. 2003, Ap&SS, 284, 225
Turcotte, S., Richer, J., Michaud, G., Iglesias, C. A., & Rogers, F. J. 1998, ApJ, 504, 539
Vidal, C. R., Cooper, J., & Smith, E. W. 1973, ApJS, 25, 37
Wade, G. A., Aurière, M., Bagnulo, S., et al. 2006, A&A, 451, 293
Weiss, W. W. 2006, in ESA SP, 1306, 93 (see Baglin 2006)